Arabian Journal of Chemistry (2016) xxx, xxx–xxx

King Saud University

Arabian Journal of Chemistry

www.ksu.edu.sa
www.sciencedirect.com

ORIGINAL ARTICLE

Reactive adsorption of toxic organophosphates parathion methyl and DMMP on nanostructured Ti/Ce oxides and their composites

Jiří Henych [a,b,*], Pavel Janoš [b], Martin Kormunda [c], Jakub Tolasz [a,c], Václav Štengl [a]

[a] Materials Chemistry Department, Institute of Inorganic Chemistry AS CR v.v.i., 25068 Řež, Czech Republic
[b] Faculty of Environment, J.E. Purkyně University in Ústí nad Labem, 400 96 Ústí n. L., Czech Republic
[c] Faculty of Science, J.E. Purkyně University in Ústí nad Labem, 400 96 Ústí n. L., Czech Republic

Received 15 March 2016; accepted 4 June 2016

KEYWORDS

Reactive sorbent;
Organophosphorus compounds;
Ceria;
Titania;
DMMP;
Parathion methyl

Abstract Pure titanium and cerium oxides and their composites were prepared by the modified method of homogeneous hydrolysis with urea as the precipitating agent. The as-synthesized nanostructured oxides were examined by XRD, XPS, microscopic techniques (SEM, HRTEM), nitrogen physisorption, and vibrational spectroscopies (FTIR, Raman). Decontamination ability of the samples towards the toxic organophosphorus compounds was determined by two methods. The reactive adsorption of the warfare agent simulant Dimethyl methylphosphonate (DMMP) was observed by *in situ* FTIR spectroscopy. The degradation of the pesticide parathion methyl in a liquid medium was investigated by liquid chromatography (HPLC). Nano-ceria exhibited substantially higher degradation ability compared to nano-titania. The highest degradation efficiency was achieved with the composites with Ti:Ce 2:8 and 1:1 molar ratio. The strong interaction of Ti with Ce led to an increase of Ce^{3+} and formation of $Ti^{<4+}$ states and changed surface area and porosity which may cause improved degradation efficacy for both DMMP and parathion methyl.

1. Introduction

Various nanostructured metal oxides exhibit a capability to capture and degrade toxic organophosphorus compounds on their surfaces even at ambient temperature (Mitchell et al., 2004; Rajagopalan et al., 2002; Sheinker and Mitchell, 2002). The reactive adsorption of chemical warfare agents (CWA), their surrogates or environmental pollutants, such as pesticides, was documented on Mg (Wagner et al., 1999), Ca (Wagner et al., 2000), Ti (Rusu and Yates, 2000; Stengl et al., 2005; Trubitsyn and Vorontsov, 2005; Wagner et al.,

* Corresponding author at: Materials Chemistry Department, Institute of Inorganic Chemistry AS CR v.v.i., 25068 Řež, Czech Republic.
E-mail address: henych@iic.cas.cz (J. Henych).
Peer review under responsibility of King Saud University.

Production and hosting by Elsevier

http://dx.doi.org/10.1016/j.arabjc.2016.06.002

2012), Mn (Prasad et al., 2007), Fe (Mitchell et al., 1997; Stengl et al., 2005), Zn (Houskova et al., 2007), Al (Wagner et al., 2001), or Ce (Chen et al., 2010; Janos et al., 2014; Mitchell et al., 2004) pure oxides. This exceptional functionality of certain metal oxides stems from their porosity, high surface area, reaching hundreds m^2 per gram of the sorbent, and the unique nanostructure (Winter et al., 2009). The unusual crystal planes of the nano-crystals are formed and exposed, and a large number of edges corners and point defects can act as active sites for the adsorption and chemical reactions (Klabunde et al., 1996). So far, investigations have been confined to clarification of the mechanism of adsorption and reactivity of pure oxides (Mitchell et al., 1997; Panayotov and Morris, 2009; Rusu and Yates, 2000; Wagner et al., 1999). But only few studies aim at the mixed or doped oxides and their comparison (Henych et al., 2015; Stengl et al., 2012b, 2011).

Mixed or doped oxides are promising materials for preparing reactive sorbents, as they often exhibit unusual structural features and properties that cannot be derived from the properties of pure oxides. The structural and optical properties of Ti/Ce mixed oxides or composites prepared by various methods were elaborated in several detailed studies (Dutta et al., 2006; Gao et al., 2010; Lopez et al., 2004; Park et al., 2010; Reddy et al., 2003; Rynkowski et al., 2000). The substantial part of the works focused on their use in heterogeneous catalysis (Gao et al., 2010) due to unique redox properties (Rynkowski et al., 2000), high oxygen storage capacity (Dutta et al., 2006), and metal-support interactions (Park et al., 2010). Ti/Ce mixed oxides and composites were also studied regarding its improved photocatalytic activity (Liu et al., 2005). Nevertheless, their use in degradation of toxic organophosphates has not been reported yet.

The rapid reactive adsorption at ambient temperature may be utilized for fast destruction of the CWA stocks, for decontamination of the sensitive military technique, or even for human protection against the terrorist threats (Wagner, 2010). CWA that can be deactivated include the organophosphorus nerve agents Soman (GD), Sarin (GB), Agent VX, or the vesicant Sulphur mustard. Because of severe toxicity of such agents, Dimethyl methylphosphonate (DMMP) is a widely used model compound for the study of the interaction of the organophosphates with the surfaces (Mitchell et al., 1997; Panayotov and Morris, 2009; Rusu and Yates, 2000). Regretfully, some organophosphorus pesticides are not structurally dissimilar to the mentioned CWA and represent a significant risk to humans, animals, and the environment. Parathion, malathion, and chlorpyrifos are representatives of well-known insecticides, which possess considerably high toxicity (Gupta and Kadel, 1990), act as endocrine disruptors (Lal et al., 2013), or may be carcinogenic (Lee et al., 2004). Even though their use is restricted (chlorpyrifos banned for residential use in the US in 2001, and parathion banned in Sweden, India, Japan, New Zealand, Portugal and other countries), their fate in waters, soil, and organic matter is a subject of major interest (Lalah and Wandiga, 2002; Mackay et al., 2014).

The composition and employed synthesis procedure substantially affect the degradation ability of the sorbents. The method of homogeneous hydrolysis (Subrt et al., 2006) has been proven to be suitable for the preparation of such reactive sorbents (Houskova et al., 2007; Stengl et al., 2010) by direct precipitation of highly crystalline nanostructured metal oxides from water solutions of metal salts at low temperature.

In this paper, the pure titanium and cerium oxides and their composites were prepared by the modified method of homogeneous hydrolysis with urea as the precipitating agent. Two different procedures were used to examine their degradation ability; the liquid-phase degradation of parathion methyl was followed by HPLC, and the reactive adsorption of the warfare simulant DMMP was studied by *in situ* FTIR spectroscopy. The degradation efficiencies of the pure oxides and composites were compared, and correlations between the material characteristics and degradation ability were established.

2. Materials and methods

2.1. Sample synthesis

The pure Ti and Ce oxides and their composites were prepared by the modified homogeneous hydrolysis of the metal salts with urea as the precipitating agent. Homogeneous hydrolysis was proven to be feasible for the production of various metal oxides and hydroxides with the well-developed nanostructure and considerably high surface area, and was described in detail elsewhere (Stengl et al., 2010; Subrt et al., 2006). In the original procedure, titanium oxysulphate ($TiOSO_4$) was dissolved in 2 L of hot distilled water acidified with H_2SO_4, and then diluted to 4 L and 300 g of urea was added. The heating of the solution leads to thermal decomposition of urea and a gradual pH increase in the solution. After 6 h of heating, a white precipitate of TiO_2 was formed. However, in our case, employing this synthesis led to undesired precipitation of Ce $(SO_4)_2$ instead of oxides; thus, this procedure cannot be used.

Therefore, in the case of TiO_2/CeO_2 composites the original method was modified to remove sulphate ions in synthesis as follows: Appropriate amount of $TiOSO_4$ (30 g for pure TiO_2) was dissolved in 2 L of hot water acidified with H_2SO_4. Then 100 mL of NH_4OH solution was continuously added to the solution while vigorously stirred, and the white precipitate was formed. This precipitate was washed with water several times to remove sulphate ions and subsequently dissolved by addition of 30 mL of nitric acid. Then a corresponding amount of $Ce(NO_3)_3{\cdot}6H_2O$ was dissolved in the solution. This mixture was diluted to a final volume (4 L), and 300 g of urea was added. Heating of the solution at 85 °C for 6 h leads to a formation of the precipitate, which was washed with water by decantation, filtered, dried, and annealed at 500 °C. The amount of starting $TiOSO_4$ and $Ce(NO_3)_3{\cdot}6H_2O$ was in Ti:Ce molar ratios 1:0 (1Ti0Ce_U), 8:2 (8Ti2Ce_U), 1:1 (1Ti1Ce_U), 2:8 (2Ti8Ce_U), and 0:1 (0Ti1Ce_U).

2.2. Characterization methods

Diffraction patterns were collected using diffractometer Bruker D2 equipped with a conventional X-ray tube (Cu Kα radiation, 30 kV, 10 mA) and the LYNXEYE 1-dimensional detector. The XRD data were processed using DiffracPlus Topas and Eva software (Bruker AXS).

FEI Nova NanoSEM 450 scanning electron microscope (SEM) was used to examine the morphology of the samples. Typically, the powdered sample was dispersed in ethanol and treated in an ultrasonic bath for 10 min before deposition on the silicon wafer chip.

FEI Talos F200X High-resolution transmission electron microscope (HRTEM) was used for structure and morphology analyses. The microscope was equipped with Super-X EDS system with four silicon drift detectors (SDDs). The samples were deposited on the 300 mesh regular copper grid.

The surface area (BET) and porosity (BJH) of samples were determined using nitrogen physisorption method with a Coulter SA3100 (Beckman) instrument.

The Raman spectra were acquired with DXR Raman microscope (Thermo Scientific). 32 two-second scans were accumulated with laser 532 nm (6 mW) under the 10× objective of Olympus microscope.

Please cite this article in press as: Henych, J. et al., Reactive adsorption of toxic organophosphates parathion methyl and DMMP on nanostructured Ti/Ce oxides and their composites. Arabian Journal of Chemistry (2016), http://dx.doi.org/10.1016/j.arabjc.2016.06.002

Infrared spectra were recorded on Thermo Nicolet NEXUS 670 FTIR spectrometer in region 4000–500 cm^{-1} with the Praying Mantis (Harrick) diffuse reflection (DR) accessory.

X-ray photoelectron spectroscopy (XPS) measurements were performed using a SPECS PHIBOS 100 hemispherical analyzer with a 5-channel detector and a SPECS XR50 X-ray source equipped with an Al and Mg dual anode. The calibration of the binding energy (BE) was performed using the C 1s main component set to 285 eV. Survey spectra were recorded with pass energy of 40 eV, and the high-resolution spectra were recorded as the sum of 10 acquisitions with a pass energy of 10 eV. A Shirley background profile was used for data processing in CasaXPS software.

Concentrations of parathion methyl and 4-NP were determined by the LaChrom HPLC system (Merck/Hitachi). The system consisted of an L-7100 pump, L-7400 variable wavelength UV/Vis detector operating at 230 nm, Rheodyne 7725i injection valve with 20 μL sampling loop, and the Luna column (Phenomenex, Torrance, CA, USA) 150 mm × 4.6 mm, packed with PFP stationary phase, 5 μm. The mixture methanol (HPLC-grade, Labscan, Dublin, Ireland)/water 80/20 (v/v), at a flow rate 1 mL min^{-1} was used as mobile phase.

2.3. Degradation test for parathion methyl

The testing procedure was described in detail in several previous studies (Janos et al., 2014; Stengl et al., 2011). The constant amounts of the sorbent (50 mg) were dispersed in 400 μL of heptane in a series of glass vials. Then a pesticide solution (100 μL, 10.000 mg L^{-1}) in heptane was added to vials (= 1 mg of the pesticide/50 mg of sorbent). The vials were sealed and covered to protect the reaction mixture from sunlight. The reaction was terminated by an addition of propan-2-ol (2 mL) at pre-determined time intervals (0.5, 8, 16, 32, 64, 96, and 128 min). The sorbent was separated by centrifugation (4000 rpm for 7 min) and the supernatant was decanted and transferred to a 50 mL volumetric flask. The sorbent was re-dispersed in 4 mL of methanol and centrifuged again. The extraction with methanol was repeated three times. All the supernatants were combined and analysed immediately by liquid chromatography (HPLC).

2.4. Reactive adsorption of DMMP

The behaviour of the liquid DMMP on the surfaces of prepared samples at ambient temperature was observed by FTIR diffuse reflectance spectroscopy (DRIFTS) using Thermo Nicolet NEXUS 670 FTIR spectrometer. In a typical experiment, the powder sample (50 mg) was placed in a DR cuvette (Praying Mantis, Harrick) and a droplet (7 μl) of a liquid DMMP (97%, Sigma–Aldrich) was dosed by an automatic micropipette. The acquisition of spectra was started immediately and repeated in selected time intervals $(0, 2, 5, \ldots n + 5$ until $30, \ldots n + 10$ until $60, \ldots n + 20$ until $120, \ldots n + 40$ until 240 min, and after 24 h). The one spectrum consists of 128 scans with acquisition time 1.48 min and resolution of 4 cm^{-1}. The spectra were baseline corrected without smoothing. All the presented spectra and kinetic curves, representing integrated peak area as a function of time, were processed using OMNIC Spectra (version 8.3) software.

3. Results and discussion

3.1. Material characterization

The XRD patterns (Fig. 1) of the as-prepared titania (1T0Ce_U) and ceria (0Ti1Ce_U) contain only diffraction lines of anatase TiO_2 and cubic CeO_2, respectively. The modification of the synthesis (removing sulphates from the reaction mixture) has been proven as feasible for a preparation of pure oxides without undesired contamination. The relatively low intensity and broadening of the lines indicated small primary crystallites of the samples, which is typical for homogeneous hydrolysis using urea as the precipitating agent (Subrt et al., 2006). In the case of TiO_2/CeO_2 composites, the sample with Ti:Ce molar ratio 2:8 (2Ti8Ce_U) had all typical diffraction lines of cubic CeO_2 with one additional line assigned to anatase TiO_2. Similarly, the equivalent molar ratio of starting Ti and Ce precursors (1Ti1Ce_U) led to a formation of two-phase system TiO_2—CeO_2. The sample with the small amount of Ce (8Ti2Ce_U) exhibited substantially broadened low-intensity lines of anatase without distinct lines of CeO_2. The semi-quantitative phase analysis, crystallite size estimation and lattice parameters obtained from Rietveld refinement are listed in Table 1. Evidently, the mixing of Ti/Ce oxides led to a reduction in mean crystallite size of both titania and ceria. The strong interaction of Ti with Ce ions in composites is further manifested in changes of lattice parameters; note a gradual increase in cell parameter c of anatase (see Table 1).

Raman spectroscopy is a sensitive probe for the phase analysis, evaluation of unit cell distortion, and the variations in the elemental environment of the nanostructured inorganic compounds (Siu et al., 1999). The results of the analysis (Fig. 2) correspond well with XRD. The typical Raman bands in positions 144 cm^{-1} (E_g), 197 cm^{-1} (E_g), 397 cm^{-1} (B_{1g}), 516 cm^{-1} (B_{1g} + A_{1g}), and 640 cm^{-1} (E_g) confirmed pure anatase in sample 1Ti0Ce_U. A strong band at position 463 cm^{-1} (sample 0Ti1Ce_U) belongs to F_{2g} mode of cubic CeO_2 structure (space group Fm-3m); the appearance of the less prominent broad bands at ca 256 cm^{-1} and 600 cm^{-1} is related to displacement of the oxygen atoms from their ideal fluorite lattice

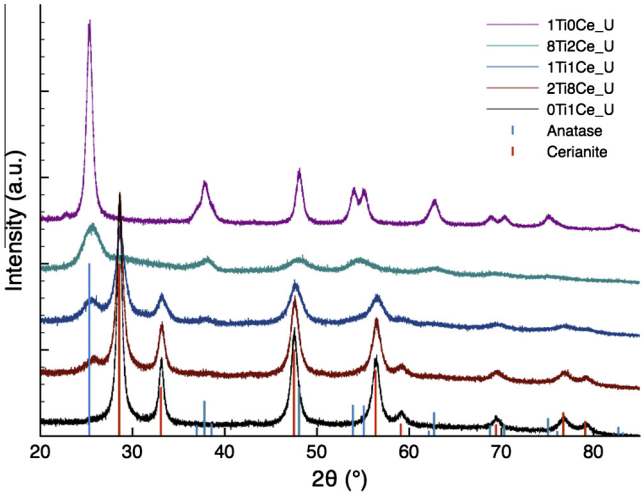

Figure 1 XRD patterns of the prepared Ti/Ce oxides.

Table 1 Sample theoretical composition (mol ratio), specific surface area (A_{BET}), total pore volume (V_{tot}), and micropore surface area ($M_{t\text{-plot}}$) determined by low temperature nitrogen physisorption and structural parameters obtained from Rietveld refinement of XRD data for synthesized Ti/Ce oxides.

Sample	Ti/Ce	A_{BET}, m^2/g	V_{tot}, cm^3/g	$M_{t\text{-plot}}$, m^2/g	TiO_2/CeO_2 (XRD), %	TiO_2 (anatase)			CeO_2 (cerianite)	
						Cryst. size, nm	Cell par. *a*, nm	Cell par. *c*, nm	Cryst. size, nm	Cell par. *a*, nm
1Ti0Ce_U	1:0	97	0.20	–	100/0	31.9	3.786	9.509	–	–
8Ti2Ce_U	8:2	146	0.36	–	65/35	12.7	3.805	9.528	1.1	5.430
1Ti1Ce_U	1:1	117	0.30	4	53/47	7.2	3.772	9.636	6.7	5.405
2Ti8Ce_U	2:8	104	0.21	8	35/65	8.7	3.748	9.698	10.2	5.411
0Ti1Ce_U	0:1	76	0.07	16	0/100	–	–	–	12.8	5.414

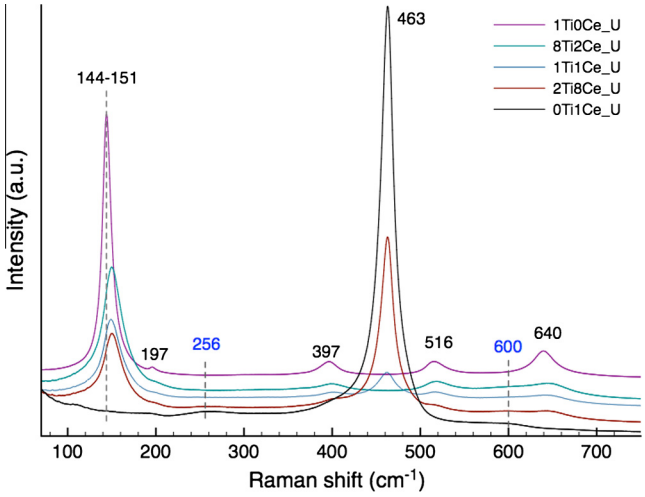

Figure 2 Raman spectra of the prepared Ti/Ce oxides.

positions and to defect-induced longitudinal optical mode (LO) of ceria caused by formation of the oxygen vacancies, respectively (Sellick et al., 2013; Tiseanu et al., 2014; Zhang et al., 2006). The sample 2Ti8Ce_U with the small amount of Ce exhibited only bands assigned to anatase TiO_2, which may indicate Ce incorporation in TiO_2 lattice. The samples with Ti/Ce molar ratios 1:1 and 2:8 contained vibrational bands of both anatase and ceria proving the formation of the two-phase composite system. Nevertheless, the strong interaction between Ti and Ce ions and distortion of the structure resulted in a significant gradual shift of the main anatase band from 144 cm^{-1} (sample 1Ti0Ce_U) to 151 cm^{-1} (sample 2Ti8Ce_U).

Diffuse infrared Fourier transform (DRIFT) spectra of the pure titania (see Fig. S1 in the supplementary material) contain only broad band centred at about 3440 cm^{-1} and band at 1631 cm^{-1}, which were assigned to ν(OH) stretching and δ (OH) bending of adsorbed water and surface hydroxyl groups. With increasing amount of Ce the new bands appeared in the samples at positions ~1510 cm^{-1}, 1317 cm^{-1}, and 1054 cm^{-1} assigned to surface bounded carbonates, which are likely to be formed on CeO_2 surfaces upon CO_2 adsorption from ambient air (Li et al., 1989; Vayssilov et al., 2011). No other remnants from the synthesis i.e. nitrates or sulphates were registered.

The surface area (A_{BET}) and total pore volume (V_{tot}) of the samples obtained from nitrogen physisorption (see Table 1) differ substantially between pure oxides and TiO_2/CeO_2 composites. Pure ceria had the lowest both surface area (76 $m^2\,g^{-1}$) and pore volume (0.07 $cm^3\,g^{-1}$). Pure titania possessed slightly higher surface area 97 $m^2\,g^{-1}$ and almost three times as large pore volume 0.2 $cm^3\,g^{-1}$. Surprisingly, in the TiO_2/CeO_2 composites increasing amount of Ti leads to a gradual increase in the surface area and pore volume. The composite with the highest amount of Ti (8Ti2Ce_U) possessed the highest A_{BET} = 146 $m^2\,g^{-1}$ and V_{tot} = 0.36 $cm^3\,g^{-1}$. The co-precipitation of CeO_2 and TiO_2 in close intimacy led to the inhibition of their crystallization, which consequently resulted in decrease in the crystallite sizes (see XRD results above). This also reflected in increased surface area and pore volume and also in significantly changed pore size distribution (Fig. 3). Pure ceria had relatively low porosity with the narrow size distribution of pores <4 nm with a contribution of micropores (see Table 1). Pure titania had larger pores in range ca 2–7 nm with the substantially higher volume of adsorbed gas. Interestingly, the mixing of TiO_2 with CeO_2 led to a significant change in the pore distribution and amount of adsorbed gas. The largest pore distribution (mesopores of ca 6–12 nm) had samples with the equivalent and 2:8 Ti:Ce molar ratio, respectively. Significantly higher pore volume than all other samples had the sample with a moderate amount of Ce (8Ti2Ce_U). The gradual increase of Ce in sample changed the hysteresis loop from type H4 of ceria (often associated with

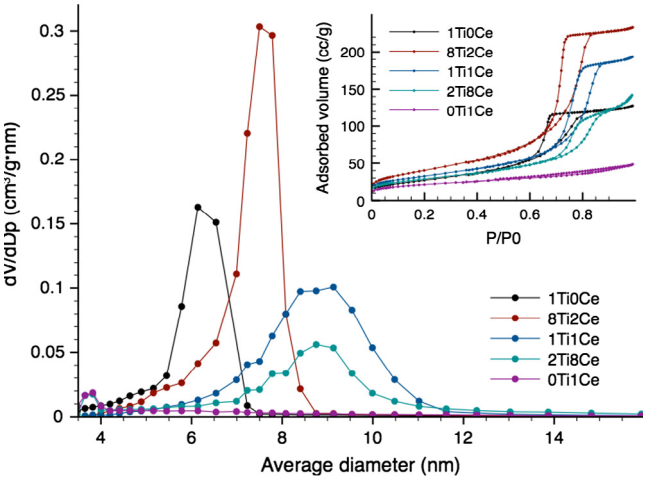

Figure 3 The pore size distribution and isotherms (inset) of the prepared Ti/Ce samples obtained from the nitrogen physisorption.

slit-like pores) to type H2 of titania, which may result from ink-bottle-like pores of varying radius, generated by agglomerates or compacts of spherical particles of non-uniform size and arrangements (Adelkhani et al., 2011).

The XPS data provided valuable information about the surface chemical states of Ti, Ce, and O and their interactions in TiO_2/CeO_2 composites. The electronic structure of CeO_2 is characterized by unoccupied 4f states of Ce^{4+} ($4f^0$) while Ce^{3+} has an occupied $4f^1$ configuration. The different 4f configurations for Ce^{4+} and Ce^{3+} result in different core levels and also valence bands. The XPS spectrum of partially reduced cerium in Ce 3d consists of three 3d3/2–3d5/2 spin-orbit-split doublets representing different $4f^0$ (Ce^{4+}) configurations in the final photoemission state and two other doubles of $4f^1$ (Ce^{3+}) states. In more detail (Fig. 4a), the highest binding energy peaks *u‴* and *v‴* (green), located at about 916.5 eV and 898.0 eV, respectively, result from the Ce $3d^9$ $4f^0$ O $2p^6$ final state. The satellite peak *u‴* associated with the Ce 3d3/2 is characteristic of the presence of Ce^{4+}. The lowest binding energy states (blue), *u* (901.0 eV), *v* (882.2 eV), *u″* (907.0 eV), and *v″* (888.5 eV), respectively, are the results of the Ce $3d^9$ $4f^2$ O $2p^4$ and Ce $3d^9$ $4f^1$ O $2p^5$ final states (Masek et al., 2009). The Ce^{3+} oxides have Ce 3d3/2 and Ce 3d5/2 spectra composed of two multiplets. The highest binding energy peaks (dark yellow), *u′* (902.9 eV) and *v′* (884.9 eV), belong to the Ce $3d^9$ $4f^1$ O $2p^6$ final state. The lower binding energy states (red), u^0 and v^0 respectively located at 899.0 eV and 880.6 eV, correspond to Ce $3d^9$ $4f^2$ O $2p^5$ final state. Practically identical components were observed in the TiO_2/CeO_2 mixed sample (see Fig. S2a in the supplementary material), but the calculated Ce^{4+}/Ce^{3+} ratio decreased by the addition of Ti from 4.8 to 4.0. Therefore, the increase in a relative number of Ce^{3+} is observed (see Table 2). The pure TiO_2 sample had single Ti 2p3/2 peak located at BE 458.9 eV which corresponds to TiO_2 state (Fig. 4b). However, the Ti 2p doublet in sample 1Ti1Ce_U (Fig. 4c) was significantly shifted to a lower BE 459.7 eV, which suggests the strong interaction of Ti with Ce and subsequent reduction in the Ti states. The peak was tentatively deconvoluted to single peaks, where ca. 37% of Ti remained in TiO_2 state (BE 458.9 eV), and about 63% of Ti has been transformed to sub-stoichiometric $Ti^{x<4+}$ oxides with BE ca 457.7 eV and 456.2 eV, respectively. The dominant single O 1s peak at BE 529.1 eV of pure ceria (Fig. 4d) represents CeO_2 (Ce^{4+}), while the second peak with a lower intensity centred at ~531.1 eV was associated with Ce^{3+} ions (Beche et al., 2008). A shoulder at higher BE (532.1 eV) was related to hydroxyl (—OH) groups on the surface of the sorbent. The O 1s peak of the pure titania (Fig. S2b) consists of dominant peak related to Ti^{4+} (BE 529.8 eV) and a shoulder at higher BE (531.2 eV) related to the surface (—OH) groups. In TiO_2/CeO_2 composite, a single broad peak was tentatively deconvoluted according to several expected components (Fig. S2c). The sample composition is presented in Table 2. Only Ti, Ce, O, and C are present on the surface of samples;

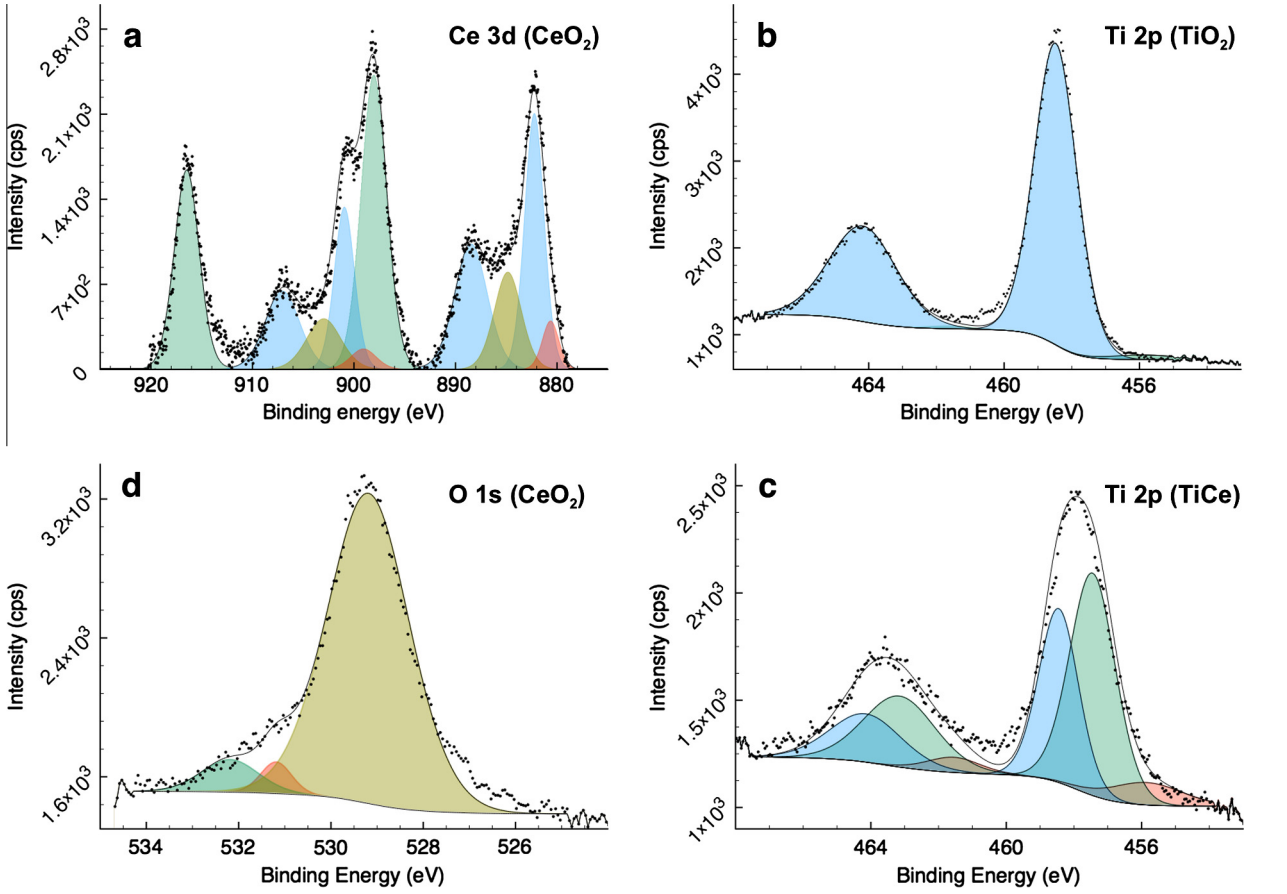

Figure 4 XPS spectra of the (a) Ce 3d region of ceria (0Ti1Ce_U), (b) Ti 2p region of pure titania (1Ti0Ce_U), (c) Ti 2p region of 1Ti1Ce_U composite, (d) O 1s region of pure ceria.

Table 2 Sample surface composition and calculated Ce^{3+}/Ce^{4+} ratio obtained from XPS.

Sample	C, %	O, %	Ti, %	Ce, %	Ce		
					Ce^{3+}, %	Ce^{4+}, %	Ce^{4+}/Ce^{3+}
1Ti0Ce_U (TiO_2)	15.1	60.6	24.3	–	–	–	–
0Ti1Ce_U (CeO_2)	12.9	64.7	–	22.3	17.3	82.7	4.8
1Ti1Ce_U	11.9	62.8	18.1	7.3	19.8	80.2	4.1

note that the lowest carbon pollution was on TiO_2/CeO_2 composite. The overall survey spectra of the TiO_2/CeO_2 sample measured using Al and Mg anodes are presented in Fig. S2d.

SEM investigation showed that ceria (sample 0Ti1Ce_U, Fig. 5a) formed micron-sized platelets clumped to flower-like agglomerates. Contrarily, titania (sample 1Ti0Ce_U, Fig. 5b) consist of small primary nanoparticles which constitute to irregular "foam" clusters. That is attributed to modification of the synthesis route since standard urea precipitation of $TiOSO_4$ provides regular mono-dispersed spherical agglomerates of primary nanoparticles (Bakardjieva et al., 2005). This confirmed that the anion of the starting metal precursor significantly affects the crystallisation process, and removing of the sulphate ions, in our case, led to the irregular morphology of precipitated titania particles. The mixing of a moderate amount of Ti with Ce precursor (sample 2Ti8Ce_U, Fig. 5c) led to a formation of two phases. However, the morphology of ceria flower-like particles is seriously disrupted, suggesting again, strong interaction of Ti with Ce. In the case of the equivalent amount of Ti and Ce (1Ti1Ce_U, Fig. 5d) and higher Ti concentration (not shown) there are hardly recognizable two distinct phases, and both ceria and titania formed irregular structure resembling foam.

TEM analysis of both titania (Fig. S3a and 3b) and ceria (Fig. S3c and 3d) showed that the agglomerates observed on SEM consist of randomly oriented nano-sized primary particles, which are smaller in the case of ceria. Also, the TiO_2/CeO_2 composite (1Ti1Ce_U, Fig. 6) had a relatively uniform structure of agglomerated nanoparticles with mean sizes ~6 to 8 nm which is coherent with calculated sizes from XRD (Table 1). There are no distinct two phases, but the EDS mapping (Fig. 6b) revealed very homogeneous dispersion of Ti and Ce in the nanostructure of the sample. This confirmed easy and efficient mixing of the elements using our modified procedure. The interplanar distances 0.32 nm (Fig. 6b) and 0.28 nm (Fig. 6c) are typical for (1 1 1) and (2 0 0) planes, respectively, of cubic ceria.

3.2. Degradation of parathion methyl

Experimental dependencies for the degradation of parathion methyl were evaluated using the following equation, that was successfully applied for the description of the CWA degradation on reactive sorbents (Stengl et al., 2012a):

$$q_t = q_1 e(-k_1 t) + q_2 e(-k_2 t) + q_\infty \quad (1)$$

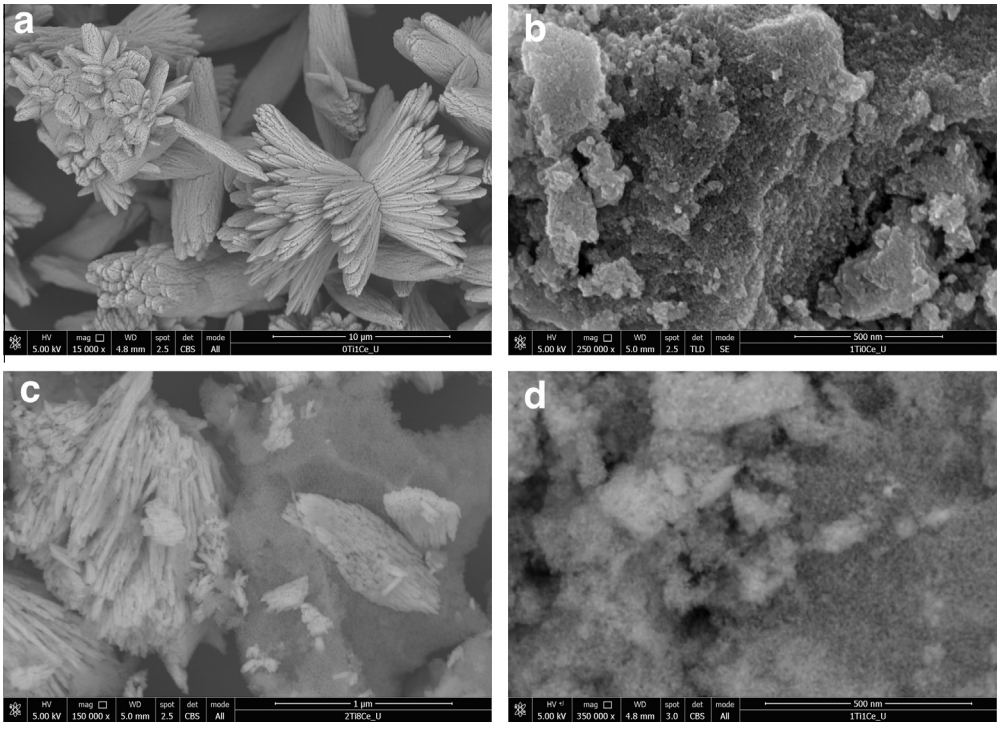

Figure 5 SEM micrographs of (a) ceria (0Ti1Ce_U), (b) titania (1Ti0Ce_U), (c) composite 2Ti8Ce_U, (d) composite 1Ti1Ce_U.

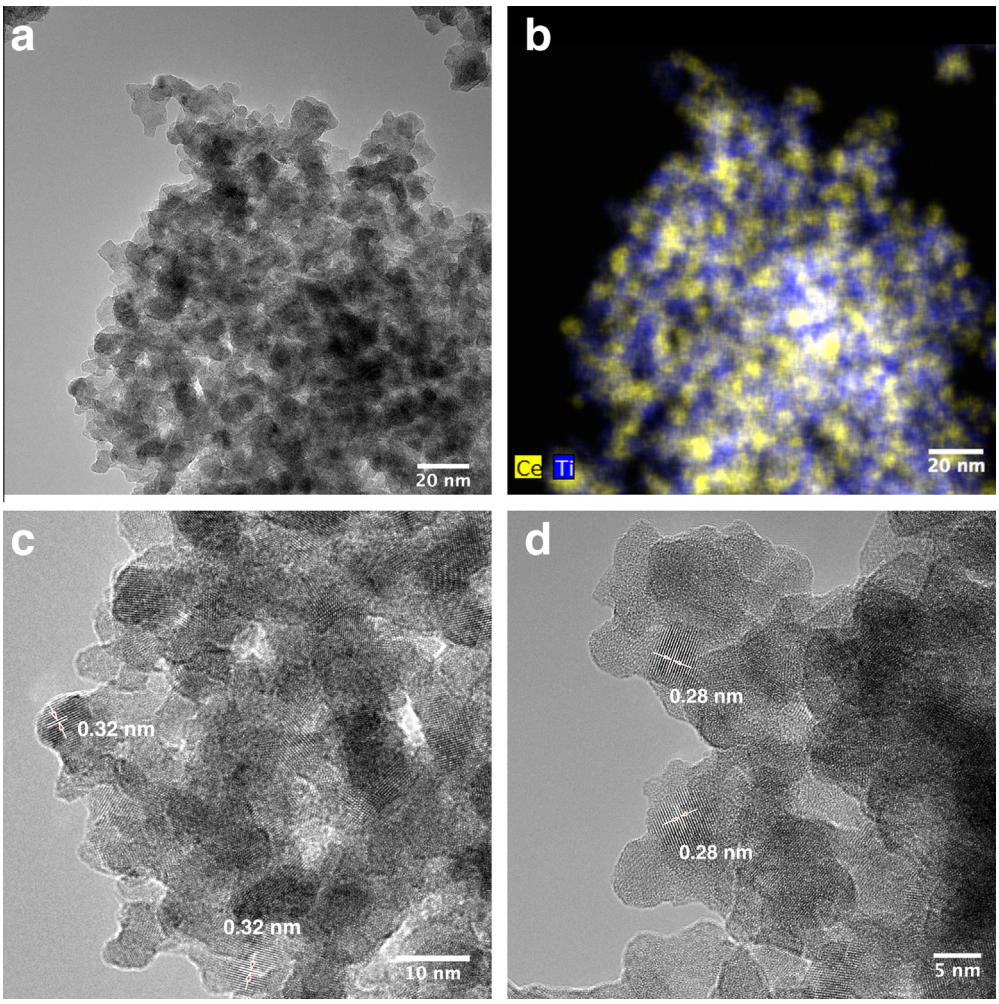

Figure 6 TEM micrographs of (a) 1Ti1Ce_U, (b) EDS map of the same place as in (a), (c and d) high-resolution TEM of the same sample.

It is assumed in this model that two processes (faster and slower) are effective in the pesticide degradation (Stengl et al., 2012a). q_t is the residual amount of pesticide in time t, k_1 and k_2 are the pseudo-first order rate constants, q_1 and q_2 are model parameters expressing the ratio, in which the faster and slower processes are involved, and q_∞ is the residual (undestroyed) amount of pesticide in infinite time. Under analogous assumptions, an equation describing the creation of 4-nitrophenol may be written as follows:

$$q_t = 1 - q'_1 e(-k'_1 t) - q_2 e'(-k'_2 t) - q'_\infty \quad (2)$$

with a similar meaning of the symbols. The model parameters obtained by nonlinear regression are listed in Table 3.

The normalised degradation curves for parathion methyl (red squares) and curves for a production of the main degradation product 4-NP (blue squares) on Ti/Ce pure oxides and their composites are presented in Fig. 7. Although the degradation of organophosphorus compounds, such as DMMP, on the surface of TiO_2 without illumination was described (Rusu and Yates, 2000), titania prepared by modified homogeneous hydrolysis was almost inactive in degradation of parathion methyl as seen in Fig. 7a. In opposite, nano-ceria prepared by our procedure proved ability to degrade parathion methyl (ca. 50% of parathion methyl was degraded in 80 min) and produce an equivalent amount of 4-NP as the primary degradation product (Fig. 7b).

It is widely accepted that the surface sites, such as corners, edges, impurities or point defects, and surface hydroxyl (—OH) groups, are responsible for reactive adsorption of the organophosphorus compounds on the nano-sized metal oxides (Chen et al., 2010; Klabunde et al., 1996). The XPS results (see above) showed that both titania and ceria contain a considerable amount of the surface hydroxyl groups on their surfaces. Nevertheless, the IR results (Fig. S1) suggested that the relative amount of adsorbed water and surface hydroxyl groups is higher on ceria. The (—OH) group is a strong nucleophile that attacks the phosphorus atom (Chen et al., 2010), which consequently leads to degradation of the parathion methyl to intermediates (i.e. 4-NP). Thus, the higher abundance of these groups on ceria may contribute to its better performance. However, the good degradation efficacy of ceria compared to titania stems from several aspects. The abundance of Ce^{3+} cations in the unique structure of ceria is compensated by the presence of oxygen vacancies. Ab initio simulation techniques suggest that the oxygen vacancies act as active sites for water dissociation (Molinari et al., 2012). The degree of

Table 3 Parameters of the kinetic models.

Sample	Degradation of parathion methyl					Creation of 4-nitrophenol				
	k_1 (min^{-1})	k_2 (min^{-1})	Initial rate of conversion[d] (μmol min^{-1})	Degree of conversion (%)	R^2	k'_1 (min^{-1})	k'_2 (min^{-1})	Initial rate of conversion[d] (μmol min^{-1})	Degree of conversion (%)	R^2
1Ti0Ce	0.110[a] (0.331)	0.010 (0.149)	0.287	7.95	0.597	N[b]	N[b]	0.023	8[c]	0.993
8Ti2Ce	N[b]	N[b]	0.093	30[c]	0.769	0.0004 (0.0025)	0.069 (0.459)	0.339	50[c]	0.998
1Ti1Ce	0.022 (0.016)	0.311 (0.452)	3.24	71.2	0.971	0.431 (0.754)	0.019 (0.008)	3.61	80[c]	0.983
2Ti8Ce	0.012 (0.005)	0.669 (0.139)	9.84	78.2	0.994	0.015 (0.008)	0.265 (0.113)	4.36	80[c]	0.994
0Ti1Ce	0.0004 (0.0005)	0.095 (0.001)	1.27	58[c]	0.985	0.073 (0.077)	0.014 (0.041)	1.28	75[c]	0.987

[a] Standard errors given in parentheses.
[b] Curve-fitting procedure does not give reasonable outputs.
[c] Estimated from the experimental curves.
[d] Calculated from the derivatives of the experimental curves at $t = 0$.

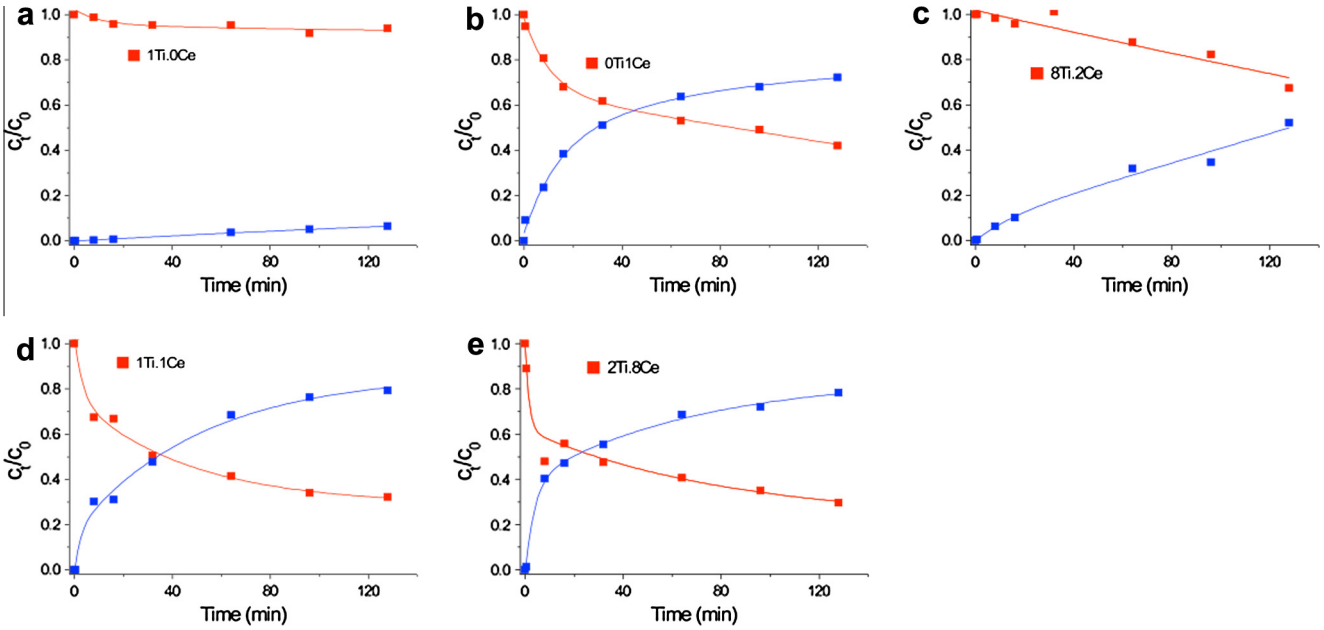

Figure 7 Degradation of parathion methyl on the sorbents (a) titania (1Ti0Ce_U), (b) ceria (0Ti1Ce_U), (c) 8Ti2Ce_U, (d) 1Ti1Ce_U, (e) 2Ti8Ce_U.

reduction in the surface is, therefore, an important parameter for the reactive adsorption of pollutants.

Interestingly, the degradation efficiency of the TiO_2/CeO_2 composites is moderately higher than that of pure CeO_2. As can be seen from Table 3, the highest degree of conversion was achieved with TiO_2/CeO_2 samples with the prevalent amount of Ce (2Ti8Ce_U, Fig. 7e) and the equivalent amount of Ce and Ti (1Ti1Ce_U, Fig. 7d) in the structure. Moreover, the initial rate of conversion is substantially higher on these two samples pointing out to their better overall reactivity towards PM. As shown in XPS results, the strong interaction of Ce with Ti leads to a partial reduction of Ti^{4+} ions and a slight increase of Ce^{3+}/Ce^{4+} ratio. The reduced sites then can act as the active sites for pesticide degradation. It implies that by the composition of the Ti/Ce mixed sample can, to some extent, control the degree of reduction in the surface and consequently the efficiency of the reactive sorbent.

Note that the TiO_2/CeO_2 composites possessed higher surface area (Table 1) and considerable wider pore size distribution (Fig. 3) compared to pure ceria and titania, which may contribute to their better performance. Nevertheless, the sample with the highest surface area and pore volume (8Ti2Ce_U) exhibited lower efficacy compared to pure ceria. Therefore, the surface area is not likely the sole parameter controlling the sorbent performance.

The most active prepared TiO_2/CeO_2 composite (rate constant $k = 0.669\ min^{-1}$) was substantially more efficient in PM degradation than TiO_2/FeO_2 composites (rate constant

$k = 0.026\ \text{min}^{-1}$) (Henych et al., 2015), and almost as active as Manganese (IV) oxide (rate constant $k = 0.888\ \text{min}^{-1}$) (Stastny et al., 2016) using similar synthesis procedure and identical testing procedure.

3.3. Reactive adsorption of DMMP

The behaviour of the nerve agent simulant DMMP vapour on the metal oxide surfaces at various temperatures was extensively studied during the last two decades (Chen et al., 2010; Mitchell et al., 2004, 1997; Panayotov and Morris, 2009; Rusu and Yates, 2000; Trubitsyn and Vorontsov, 2005). In this work, a liquid DMMP, without subsequent UV or Vis illumination at ambient temperature, was used as a model compound to study the reactivity of the metal oxide surfaces. The obtained DRIFT fingerprint spectra of the DMMP reactive adsorption on selected Ti/Ce oxides in various time intervals are presented in Fig. 8. Tentative assignment of the bands was made according to the literature (Moss et al., 2005; Rusu and Yates, 2000). The adsorption of DMMP is realized through binding of the electron-rich phosphoryl oxygen (P═O) to the surface at either Lewis acid sites or with hydroxyl groups by hydrogen-bond formation. For temperatures higher than 200 K is the adsorption dissociative, leading to the formation of an adsorbed non-volatile methyl methylphosphonate passivating the adsorption sites, while the second methyl group presumably forms methanol (Mitchell et al., 2004; Rusu and Yates, 2000).

Thus, the fate of P═O vibration may indicate the reactivity of the sorbent surface. The P═O stretching vibrations of DMMP gas occur at $1276\ \text{cm}^{-1}$ (Rusu and Yates, 2000), whereas in a liquid phase (measured by ATR technique) it were found at $\sim 1260\ \text{cm}^{-1}$. The surface adsorption should lead to further downshift of the wavenumber. The P═O vibration of DMMP on the surface TiO_2 (Fig. 8a) measured immediately upon application (time 0) was found at $\sim 1265\ \text{cm}^{-1}$. After 15 min, the only change in the spectra is downshift of the bands, as DMMP is being bounded the surface; however, no significant change in intensity was observed. The P═O band is further downshifted in the course of reaction suggesting the strong interaction of DMMP with the surface. After 24 h, the P═O band was found at $1233\ \text{cm}^{-1}$, but only slightly changed in intensity, that is consistent with the degradation of PM (see above), which suggests the very low activity of as prepared titania for organophosphates decomposition. Contrarily, when DMMP was applied onto ceria surface

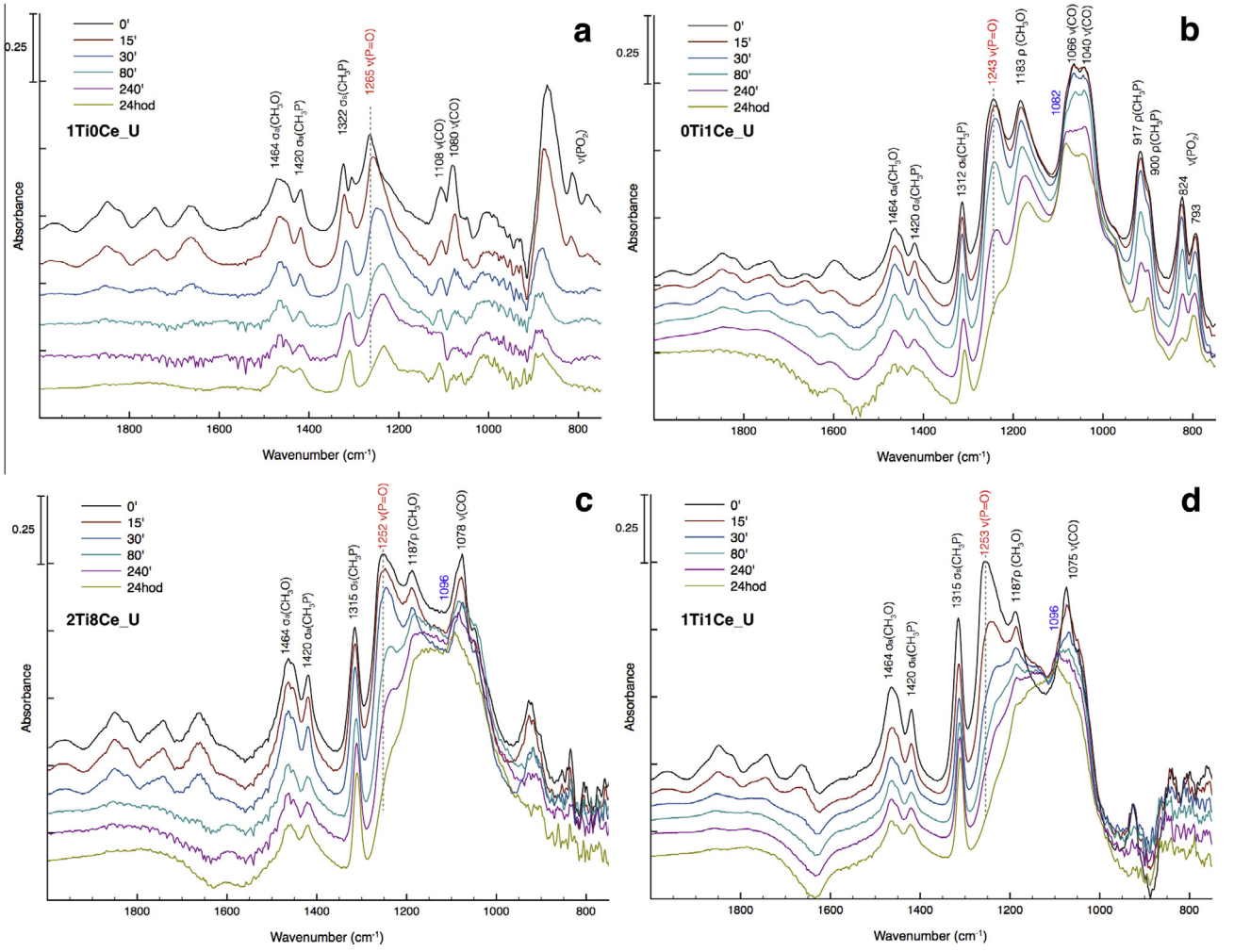

Figure 8 Fingerprint DRIFT spectra of DMMP reactive adsorption on selected Ti/Ce samples. (a) titania (1Ti0Ce_U), (b) ceria (0Ti1Ce_U), (c) 2Ti8Ce_U, (d) 1Ti1Ce_U.

(Fig. 8b), the P═O band was registered at 1243 cm^{-1}, which corresponds to surface adsorbed DMMP and which is 20 cm^{-1} downshifted compared to titania. This suggests that DMMP is much faster adsorbed on ceria surfaces. Furthermore, the P═O band progressively lose its intensity, which is accompanied with emerging of a new O─P─O band at 1082 cm^{-1}. As the reactive adsorption took place, the P═O double bond is being transformed to O─P─O species, which has an intermediate character between a single and double bond (Rusu and Yates, 2000). As a consequence is expected that all other bands (P─O, C─O, C─P) will be influenced. The shoulder of P═O band is still clearly visible even after 24 h, which indicates that all available active sites for DMMP were used, and no further DMMP can be transformed. In the case of TiO_2/CeO_2 composites with the prevalent amount of Ce (2Ti8Ce_U, Fig. 8c) and the equivalent amount of Ti and Ce (1Ti1Ce_U, Fig. 8d) the P═O vibration was found at 1252 cm^{-1} and 1253 cm^{-1}, respectively. These values lie somewhat between those found for pure ceria and titania, which correspond to the combination of TiO_2 and CeO_2 in the sample. After 15 min the P═O band downshifted to 1245 cm^{-1} and decreased in intensity as the P═O band undergoes transformation. This trend continues with prolonged time and a new band assigned to O─P─O species appeared at 1096 cm^{-1}. Note the decrease in intensity of the other bands (C─O and CH_3O), while the bands related to CH_3P remain very stable. This may indicate dissociation of DMMP, including liberation of the methoxy groups, to the final surface product methyl methylphosphonate. The kinetics of disappearance of the P═O band (calculated from the integrated peak area), as a main indication of the reactive adsorption, is presented in Fig. S3. As can be seen, the TiO_2/CeO_2 composites (2Ti8Ce_U, 1Ti1Ce_U) were more efficient in the elimination of the P═O band compared to pure ceria. These results are consistent with the results of PM degradation (see above).

The DRIFT spectra of the CH stretching region of the selected samples are presented in supplementary Fig. S4. As can be seen, the intensities of the CH_3 bands on the surface of titania (Fig. S4a) are substantially lower than those on pure ceria (Fig. S4b) and TiO_2/CeO_2 composites (Fig. S4c and S4d). Therefore, much less of DMMP is being adsorbed on titania. With prolonged time, the intensities of CH_3 bands on all samples decreased as methoxy species are liberated from DMMP molecule. The normalised curves describing the change in the sum of all CH groups as a function of time can be seen in Fig. S5. Their decrease in time is correlated with degradation of the P═O band and suggests the overall reactivity of the sorbent surfaces.

4. Conclusions

The Ti/Ce pure oxides and their composites were successfully prepared by the modified homogeneous hydrolysis with urea as the precipitating agent. The step of removing sulphate ions in synthesis led to a significant change in the aggregation of primary particles and changed the morphology of titania micro-aggregates from sphere-like to irregular "foam". Ti and Ce ions significantly interact in composite samples, and close interaction between Ti and Ce led to a formation of $Ti^{<4+}$ species as shown in XPS investigation. The surface area and porosity were also substantially changed in TiO_2/CeO_2 composites compared to pure titania and ceria. The HRTEM observation revealed very good homogeneous dispersion of Ti and Ce in the nanostructure of the samples. The pure Ti/Ce oxides and composites were then tested for their degradation ability towards toxic organophosphates – pesticide parathion methyl and warfare simulant DMMP. Both tests revealed that titania was almost inactive, whereas ceria is effective in degradation of organophosphates on their surfaces. Surprisingly, the most active samples were TiO_2/CeO_2 composites with 2:8 and 1:1 Ti:Ce molar ratio. Their good degradation ability stems from the abundance of the reduced $Ti^{<4+}$ and Ce^{3+} states, which can act as active sites for PM and DMMP degradation. It implies that by the composition of the TiO_2/CeO_2 composite can be, to some extent, controlled the degree of reduction in the surface, and consequently the efficiency of the reactive sorbent. TiO_2/CeO_2 composites also possessed higher surface area and wider pores, which may contribute to better performance.

Acknowledgements

The authors thank Michaela Slušná and Zuzana Bělčická for surface area and Raman spectra measurements, respectively. MK acknowledges the support from the Czech Science Foundation project No.: 13-06989S. The support from the Internal Student Grant Agency of the J.E. Purkyně University in Ústí nad Labem (internal project number: 44201 15 0073 01) is also gratefully acknowledged.

Appendix A. Supplementary material

Supplementary data associated with this article can be found, in the online version, at http://dx.doi.org/10.1016/j.arabjc.2016.06.002.

References

Adelkhani, H., Ghaemi, M., Ruzbehani, M., 2011. Evaluation of the porosity and the nano-structure morphology of MnO_2 prepared by pulse current electrodeposition. Int. J. Electrochem. Sci. 6, 123–135.

Bakardjieva, S., Subrt, J., Stengl, V., Dianez, M.J., Sayagues, M.J., 2005. Photoactivity of anatase-rutile TiO_2 nanocrystalline mixtures obtained by heat treatment of homogeneously precipitated anatase. Appl. Catal. B – Environ. 58, 193–202.

Beche, E., Charvin, P., Perarnau, D., Abanades, S., Flamant, G., 2008. Ce 3d XPS investigation of cerium oxides and mixed cerium oxide ($Ce_xTi_yO_z$). Surf. Interface Anal. 40, 264–267.

Chen, D.A., Ratliff, J.S., Hu, X.F., Gordon, W.O., Senanayake, S.D., Mullins, D.R., 2010. Dimethyl methylphosphonate decomposition on fully oxidized and partially reduced ceria thin films. Surf. Sci. 604, 574–587.

Dutta, G., Waghmare, U.V., Baidya, T., Hegde, M.S., Priolkar, K.R., Sarode, P.R., 2006. Origin of enhanced reducibility/oxygen storage capacity of $Ce_{1-x}Ti_xO_2$ compared to CeO_2 or TiO_2. Chem. Mater. 18, 3249–3256.

Gao, X., Jiang, Y., Zhong, Y., Luo, Z.Y., Cen, K.F., 2010. The activity and characterization of CeO_2–TiO_2 catalysts prepared by the sol–gel method for selective catalytic reduction of NO with NH_3. J. Hazard. Mater. 174, 734–739.

Gupta, R.C., Kadel, W.L., 1990. Methyl parathion acute toxicity – prophylaxis and therapy with memantine and atropine. Arch. Int. Pharm. Ther. 305, 208–221.

Henych, J., Stengl, V., Slusna, M., Grygar, T.M., Janos, P., Kuran, P., Stastny, M., 2015. Degradation of organophosphorus pesticide parathion methyl on nanostructured titania–iron mixed oxides. Appl. Surf. Sci. 344, 9–16.

Houskova, V., Stengl, V., Bakardjieva, S., Murafa, N., Kalendova, A., Oplustil, F., 2007. Zinc oxide prepared by homogeneous hydrolysis with thioacetamide, its destruction of warfare agents, and photocatalytic activity. J. Phys. Chem. A 111, 4215–4221.

Janos, P., Kuran, P., Kormunda, M., Stengl, V., Grygar, T.M., Dosek, M., Stastny, M., Ederer, J., Pilarova, V., Vrtoch, L., 2014. Cerium dioxide as a new reactive sorbent for fast degradation of parathion methyl and some other organophosphates. J. Rare Earth 32, 360–370.

Klabunde, K.J., Stark, J., Koper, O., Mohs, C., Park, D.G., Decker, S., Jiang, Y., Lagadic, I., Zhang, D.J., 1996. Nanocrystals as stoichiometric reagents with unique surface chemistry. J. Phys. Chem. 100, 12142–12153.

Lal, B., Sarang, M.K., Kumar, P., 2013. Malathion exposure induces the endocrine disruption and growth retardation in the catfish, Clarias batrachus (Linn.). Gen. Comp. Endocr 181, 139–145.

Lalah, J.O., Wandiga, S.O., 2002. The effect of boiling on the removal of persistent malathion residues from stored grains. J. Stored Prod. Res. 38, 1–10.

Lee, W.J., Blair, A., Hoppin, J.A., Lubin, J.H., Rusiecki, J.A., Sandler, D.P., Dosemeci, M., Alavanja, M.C.R., 2004. Cancer incidence among pesticide applicators exposed to chlorpyrifos in the agricultural health study. J. Natl. Cancer I 96, 1781–1789.

Li, C., Sakata, Y., Arai, T., Domen, K., Maruya, K., Onishi, T., 1989. Carbon-monoxide and carbon-dioxide adsorption on cerium oxide studied by fourier-transform infrared-spectroscopy. 1. Formation of carbonate species on dehydroxylated CeO_2 at room-temperature. J. Chem. Soc. Faraday Trans. 1 85, 929–943.

Liu, Z.L., Guo, B., Hong, L., Jiang, H.X., 2005. Preparation and characterization of cerium oxide doped TiO_2 nanoparticles. J. Phys. Chem. Solids 66, 161–167.

Lopez, T., Rojas, F., Alexander-Katz, R., Galindo, F., Balankin, A., Buljan, A., 2004. Porosity, structural and fractal study of sol–gel TiO_2–CeO_2 mixed oxides. J. Solid State Chem. 177, 1873–1885.

Mackay, D., Giesy, J.P., Solomon, K.R., 2014. Fate in the environment and long-range atmospheric transport of the organophosphorus insecticide, chlorpyrifos and its oxon. Rev. Environ. Contam. Toxicol. 231, 35–76.

Masek, K., Vaclavu, M., Babor, P., Matolin, V., 2009. Sn–CeO_2 thin films prepared by RF magnetron sputtering: XPS and SIMS study. Appl. Surf. Sci. 255, 6656–6660.

Mitchell, M.B., Sheinker, V.N., Cox, W.W., Gatimu, E.N., Tesfamichael, A.B., 2004. The room temperature decomposition mechanism of dimethyl methylphosphonate (DMMP) on alumina-supported cerium oxide – participation of nano-sized cerium oxide domains. J. Phys. Chem. B 108, 1634–1645.

Mitchell, M.B., Sheinker, V.N., Mintz, E.A., 1997. Adsorption and decomposition of dimethyl methylphosphonate on metal oxides. J. Phys. Chem. B 101, 11192–11203.

Molinari, M., Parker, S.C., Sayle, D.C., Islam, M.S., 2012. Water adsorption and its effect on the stability of low index stoichiometric and reduced surfaces of ceria. J. Phys. Chem. C 116, 7073–7082.

Moss, J.A., Szczepankiewicz, S.H., Park, E., Hoffmann, M.R., 2005. Adsorption and photodegradation of dimethyl methylphosphonate vapor at TiO_2 surfaces. J. Phys. Chem. B 109, 19779–19785.

Panayotov, D.A., Morris, J.R., 2009. Uptake of a chemical warfare agent simulant (DMMP) on TiO_2: reactive adsorption and active site poisoning. Langmuir 25, 3652–3658.

Park, J.B., Graciani, J., Evans, J., Stacchiola, D., Senanayake, S.D., Barrio, L., Liu, P., Sanz, J.F., Hrbek, J., Rodriguez, J.A., 2010. Gold, copper, and platinum nanoparticles dispersed on CeO_x/TiO_2 (110) surfaces: high water–gas shift activity and the nature of the mixed-metal oxide at the nanometer level. J. Am. Chem. Soc. 132, 356–363.

Prasad, G.K., Mahato, T.H., Pandey, P., Singh, B., Suryanarayana, M.V.S., Saxena, A., Shekhar, K., 2007. Reactive sorbent based on manganese oxide nanotubes and nanosheets for the decontamination of 2-chloro-ethyl ethyl sulphide. Microporous Mesoporous Mater. 106, 256–261.

Rajagopalan, S., Koper, O., Decker, S., Klabunde, K.J., 2002. Nanocrystalline metal oxides as destructive adsorbents for organophosphorus compounds at ambient temperatures. Chem.-Eur. J. 8, 2602–2607.

Reddy, B.M., Khan, A., Yamada, Y., Kobayashi, T., Loridant, S., Volta, J.C., 2003. Structural characterization of CeO_2–MO_2 ($M = Si^{4+}$, Ti^{4+}, and Zr^{4+}) mixed oxides by Raman spectroscopy, X-ray photoelectron spectroscopy, and other techniques. J. Phys. Chem. B 107, 11475–11484.

Rusu, C.N., Yates, J.T., 2000. Adsorption and decomposition of dimethyl methylphosphonate on TiO_2. J. Phys. Chem. B 104, 12292–12298.

Rynkowski, J., Farbotko, J., Touroude, R., Hilaire, L., 2000. Redox behaviour of ceria-titania mixed oxides. Appl. Catal. A – Gen. 203, 335–348.

Sellick, D.R., Aranda, A., Garcia, T., Lopez, J.M., Solsona, B., Mastral, A.M., Morgan, D.J., Carley, A.F., Taylor, S.H., 2013. Influence of the preparation method on the activity of ceria zirconia mixed oxides for naphthalene total oxidation. Appl. Catal. B – Environ. 132, 98–106.

Sheinker, V.N., Mitchell, M.B., 2002. Quantitative study of the decomposition of dimethyl methylphosphonate (DMMP) on metal oxides at room temperature and above. Chem. Mater. 14, 1257–1268.

Siu, G.G., Stokes, M.J., Liu, Y.L., 1999. Variation of fundamental and higher-order Raman spectra of ZrO_2 nanograins with annealing temperature. Phys. Rev. B 59, 3173–3179.

Stastny, M., Stengl, V., Henych, J., Tolasz, J., Vomacka, P., Ederer, J., 2016. Mesoporous manganese oxide for the degradation of organophosphates pesticides. J. Mater. Sci. 51, 2634–2642.

Stengl, V., Houskova, V., Bakardjieva, S., Murafa, N., Marikova, M., Oplustil, F., Nemec, T., 2010. Zirconium doped nano-dispersed oxides of Fe, Al and Zn for destruction of warfare agents. Mater. Charact. 61, 1080–1088.

Stengl, V., Kralova, D., Oplustil, F., Nemec, T., 2012a. Mesoporous manganese oxide for warfare agents degradation. Microporous Mesoporous Mater. 156, 224–232.

Stengl, V., Marikova, M., Bakardjieva, S., Subrt, J., Oplustil, F., Olsanska, M., 2005. Reaction of sulfur mustard gas, soman and agent VX with nanosized anatase TiO_2 and ferrihydrite. J. Chem. Technol. Biotechnol. 80, 754–758.

Stengl, V., Matys Grygar, T., Bludska, J., Oplustil, F., Nemec, T., 2012b. Mesoporous iron-manganese oxides for sulphur mustard and soman degradation. Mater. Res. Bull. 47, 4291–4299.

Stengl, V., Matys Grygar, T., Oplustil, F., Nemec, T., 2011. Sulphur mustard degradation on zirconium doped Ti–Fe oxides. J. Hazard. Mater. 192, 1491–1504.

Subrt, J., Stengl, V., Bakardjieva, S., Szatmary, L., 2006. Synthesis of spherical metal oxide particles using homogeneous precipitation of aqueous solutions of metal sulfates with urea. Powder Technol. 169, 33–40.

Tiseanu, C., Parvulescu, V., Avram, D., Cojocaru, B., Sanchez-Dominguez, M., 2014. Exceptional capability of nanosized CeO_2 materials to "dissolve" lanthanide oxides established by time-gated excitation and emission spectroscopy. Dalton Trans. 43, 7622–7630.

Trubitsyn, D.A., Vorontsov, A.V., 2005. Experimental study of dimethyl methylphosphonate decomposition over anatase TiO_2. J. Phys. Chem. B 109, 21884–21892.

Vayssilov, G.N., Mihaylov, M., St Petkov, P., Hadjiivanov, K.I., Neyman, K.M., 2011. Reassignment of the vibrational spectra of carbonates, formates, and related surface species on ceria: a combined density functional and infrared spectroscopy investigation. J. Phys. Chem. C 115, 23435–23454.

Wagner, G.W., 2010. Decontamination of chemical warfare agents with nanosize metal oxides. ACS Sym. Ser. 1045, 125–136.

Please cite this article in press as: Henych, J. et al., Reactive adsorption of toxic organophosphates parathion methyl and DMMP on nanostructured Ti/Ce oxides and their composites. Arabian Journal of Chemistry (2016), http://dx.doi.org/10.1016/j.arabjc.2016.06.002

Wagner, G.W., Bartram, P.W., Koper, O., Klabunde, K.J., 1999. Reactions of VX, GD, and HD with nanosize MgO. J. Phys. Chem. B 103, 3225–3228.

Wagner, G.W., Koper, O.B., Lucas, E., Decker, S., Klabunde, K.J., 2000. Reactions of VX, GD, and HD with nanosize CaO: autocatalytic dehydrohalogenation of HD. J. Phys. Chem. B 104, 5118–5123.

Wagner, G.W., Peterson, G.W., Mahle, J.J., 2012. Effect of adsorbed water and surface hydroxyls on the hydrolysis of VX, GD, and HD on titania materials: the development of self-decontaminating paints. Ind. Eng. Chem. Res. 51, 3598–3603.

Wagner, G.W., Procell, L.R., O'Connor, R.J., Munavalli, S., Carnes, C.L., Kapoor, P.N., Klabunde, K.J., 2001. Reactions of VX, GB, GD, and HD with nanosize Al2O3. Formation of aluminophosphonates. J. Am. Chem. Soc. 123, 1636–1644.

Winter, M., Hamal, D., Yang, X.X., Kwen, H., Jones, D., Rajagopalan, S., Klabunde, K.J., 2009. Defining reactivity of solid sorbents: what is the most appropriate metric? Chem. Mater. 21, 2367–2374.

Zhang, F., Chen, C.H., Hanson, J.C., Robinson, R.D., Herman, I.P., Chan, S.W., 2006. Phases in ceria-zirconia binary oxide $(1-x)$ $CeO_{2-x}ZrO(2)$ nanoparticles: the effect of particle size. J. Am. Ceram. Soc. 89, 1028–1036.

Please cite this article in press as: Henych, J. et al., Reactive adsorption of toxic organophosphates parathion methyl and DMMP on nanostructured Ti/Ce oxides and their composites. Arabian Journal of Chemistry (2016), http://dx.doi.org/10.1016/j.arabjc.2016.06.002